Study of the Adsorption and Desorption of Multiple Adsorbates in a Fixed Bed

An experimental and theoretical study was made of the adsorption of ethane/propane mixtures from nitrogen or helium. The study also covered the desorption of the mixtures using a purge of hot nitrogen or helium. The adsorbent was Witco JXC activated carbon. A nonequilibrium, mechanistic model was developed and was shown to represent both adsorption and desorption processes. The model utilized mixture isotherm data predicted by the Flory Huggins form of the vacancy solution model. Both adsorption and hot purge regeneration were found to be intraparticle rate controlled processes, with surface diffusion dominating the intraparticle mass transfer mechanism. The dynamic model can be used for the simulation of a variety of commercial adsorption and desorption conditions.

Chen-Chia Huang and James R. Fair
Department of Chemical Engineering
University of Texas
Austin, TX 78712

Separation of gas mixtures by adsorption processes has been widely applied in industry. Pressure swing adsorption (PSA) and thermal swing adsorption (TSA) are the two most common adsorptive cyclic processes. The PSA system is well suited to the separation of weakly adsorbed species. For strongly adsorbed species, however, TSA is generally preferred. A TSA process includes adsorption and thermal regeneration steps, with the latter step being energy-intensive. Published studies of mechanisms associated with this process are relatively few, especially for the regeneration step and for multiple adsorbates. Accordingly, in the present study an effort was made to better understand the mechanisms of adsorption and thermal regeneration of a fixed bed with multiple adsorbates. The purposes of the research include developing a nonequilibrium model for nonisothermal, nonadiabatic multicomponent adsorption and desorption cyclic processes and collecting the pertinent experimental data. Unlike the approach of previous workers, a vacancy solution equilibrium model (VSM) was applied in the present dynamic model. The VSM is based on thermodynamic theory, and only pure component isotherm data are needed to predict mixture isotherms.

Previous Work

A number of models have been developed over the years under various simplifying assumptions. Most of them deal with only a single adsorbate. An excellent review of single-component adsorption modeling has been published recently by Schork (1986). Because of the physical complexity and the mathematical difficulty, little work with multicomponent adsorption had been reported before 1970. Recently, Yang (1987) has provided an excellent review of multicomponent adsorption, particularly based on equilibrium theory.

A summary of previous work on multicomponent adsorption is given in Table 1. In most cases, Langmuir isotherms were used. Constant pattern approximations were generally employed in order to simplify the problem and make it amenable to analytical solution. In one case (Sircar and Kumar, 1983), this approximation was extended to handle bulk binary gas mixtures in an adiabatic column. Background on the studies listed in Table 1 may be found elsewhere (Huang, 1987).

Regeneration is an important step in thermal swing adsorption and usually determines the economic success of the process. The paper by Rhee et al. (1972) may be the first publication on multicomponent desorption kinetics. These authors assumed local equilibrium at each point in the column and solved the kinetics problem by the method of characteristics. They investigated the effects of purge gas temperature as well as its composition.

Sircar and Kumar (1985) developed a local equilibrium theory for adiabatic desorption of bulk binary mixtures by isobaric purge. The purge gas, which is the mixture rich in the nonkey component, enters the column saturated with a gas mixture rich in the key component at the same pressure and temperature as the initial column conditions. Analytical equations describing isothermal desorption of bulk binary adsorbates by purging were also derived. Mixture isotherm equations of the Langmuir type

Table 1. Multicomponent Gas Adsorption Models

Researchers	Thermal Condition	Mass Transfer Resistances	Isotherm	Adsorption/ Desorption	Comments
Rhee & Amundson (1970, 1972, 1974)	Adiabatic	Local equilibrium	Langmuir	Adsorption desorption	Theoretical analysis
Thomas & Lombardi (1971)	Isothermal	Surface diffusion	Langmuir	Adsorption	Constant pattern
Gariepy & Zwiebel (1971)	Isothermal	Gas film	Langmuir	Adsorption	Method of characteristics
Cooney & Strusi (1972)	Isothermal	Solid film	Langmuir	Adsorption	Analytical solution, Constant pattern
Collins & Chao (1973)	Adiabatic	Overall (gas film + pore diffusion)	General	Adsorption desorption	Method of (1973) characteristics
Carter & Husain (1974)	Isothermal	Pore diffusion	Langmuir	Adsorption	Crank-Nicolson method
Zwiebel et al. (1974)	Isothermal	Gas film	Langmuir	Adsorption	Method of characteristics
Miura et al. (1979)	Isothermal	Gas + solid film	Langmuir, Freundlich	Adsorption	Constant pattern
Miura & Hashimoto (1979)	Isothermal	Gas film, solid film	Langmuir	Adsorption	Analytical solution, Constant pattern
Harwell et al. (1980)	Adiabatic	Overall (gas film + pore diffusion)	Langmuir	Adsorption	Method of characteristics
Wong & Neidzwiecki (1982)	Isothermal, Adiabatic	Overall (gas film + pore diffusion)	Langmuir	Adsorption	Method of lines
Sircar & Kumar (1983, 1986)	Adiabatic	Gas film, solid film	Langmuir	Adsorption	Constant pattern
Sircar & Kumar (1985)	Adiabatic	Local equilibrium	Langmuir	Desorption	Analytical solution
Nagel et al. (1987)	Adiabatic	Parallel diffusion	Langmuir	Adsorption	Collocation method
Basmadjian et al. (1987[a,b,c])	Isothermal	Local equilibrium	Type I, II, IV	Adsorption desorption	Analytical solution

were used. Basmadjian et al. (1987a, b, c) recently studied isothermal fixed-bed sorption based on equilibrium theory and different types of isotherms (Type I, II and IV).

Equilibrium theory is aimed at identifying concentration and temperature plateaus in the bed or the histories of concentration and temperature of the effluent. Since the isotherm is generally unfavorable for desorption, the mass transfer zone is dispersive. The concentration waves lead to a continuously spreading-out, in other words, in proportionate pattern behavior. Therefore, depletion curves predicted by equilibrium theory give only approximate representations of the behavior found in real systems.

Collins and Chao (1973) demonstrated the feasibility of calculating both adsorption and desorption behavior from a dynamic model for nonequilibrium, adiabatic, multicomponent systems. They calculated the mass and heat transfer rates by lumping the resistances of gas film and intraparticle diffusion. Unfortunately, no experimental data were provided for comparing the calculation results.

Zwiebel et al. (1974) presented the first generalized depletion data for multicomponent systems with nonlinear isotherms. A mathematical model was also presented with assumptions of dilute gases, isothermal operation, constant pressure, a fluid film mass transfer mechanism, and Langmuir-type isotherms. However, the system is assumed to be at about room temperature. Basmadjian and Wright (1981) first reported experimental nonisothermal multisolute desorption data without modeling. The feed temperature of the purge gas was cold and near room temperature. Neither nonisothermal multisolute thermal purge regeneration experimental data nor the related mathematical models have been reported.

On the basis of work reported, models for the adsorption step, especially for the desorption step, appear to have limitations when applied to multisolute systems. The present work was undertaken with the objective of removing these limitations.

Equilibrium Measurements

A Micromeritics Accusorb 2100E gas adsorption analyzer was used to measure isotherms of pure adsorbate (ethane and propane) on activated carbon. This instrument employs a manometric method for measurement of adsorption isotherms. The system can be placed under vacuum down to 10^{-4} mm Hg by a combination of a forepump and a diffusion pump. The system pressure is measured accurately by a pressure transducer and is displayed by a four-digit automatic-ranging indicator. During data acquisition, the adsorbent samples are held at the desired temperature by placement of sample flasks in the ovens provided with the instrument.

The Flory-Huggins form of the Vacancy Solution Model (FH-VSM) isotherm equation (Cochran et al., 1985a) for a pure adsorbate was found to fit the individual isotherm data well. The pure component isotherm equation is:

$$P = \left[\frac{w_1^\infty}{b_1}\frac{\theta}{1-\theta}\right]\exp\left[\frac{\alpha_{1v}^2\,\theta}{1+\alpha_{1v}\theta}\right] \tag{1}$$

$$w_1^\infty = w_{01}^\infty \exp\left[\frac{r_1}{T}\right] \tag{2}$$

where:

$$b_1 = b_{01}\exp\left[\frac{-\Delta H}{RT}\right] \tag{3}$$

$$\alpha_{1v} = m_1 w_1^\infty - 1 \tag{4}$$

$$\theta = \frac{w_1}{w_1^\infty} \tag{5}$$

There are five adjustable parameters (b_{01}, m_1, w_{01}^∞, r_1, and

Table 2. Parameters in the FH-VSM Pure Component Isotherm Equation

Adsorbate	w_{01}^{∞}	r_1	b_{01}	$-\Delta H$	m_1
Propane	1.355×10^{-3}	392.8	8.136×10^{-10}	4.08×10^{7}	898.6
Ethane	2.350×10^{-3}	255.0	9.973×10^{-10}	3.35×10^{7}	719.0

w_{01}^{∞} in (kmol/kg) $-\Delta H$ in J/kmol b_{01} in (kmol/kg · kPa)
r_1 in K m_1 in kg/kmol

ΔH) in the above equations. The appropriate set of constants determined by an unconstrained nonlinear programming package for each adsorbate is listed in Table 2. The correlation results are plotted along with the experimental data in Figures 1 and 2.

The limiting amount adsorbed on a unit mass of adsorbent, w_1^{∞}, and the Henry's constant, b_1, are derived from the correlated parameters as shown in Eqs. 2 and 3, respectively. However, unless the experimental data extend over the entire concentration range from the Henry's law region to near saturation, w_1^{∞} and b_1 both may not have physical significance (Ruthven, 1984). Since in the present study the isotherm data are confined to the low concentration region, the term b_1 may have physical meaning, but w_1^{∞} may not.

The pure-component isotherm equation from FH-VSM is a Langmuir-type equation (if α_{1v} is zero). The exponential term on the righthand side of Eq. 1 can be considered as a correction term. For Langmuir-type isotherms, the isosteric heat of adsorption, ΔH, is constant and is determined by the Henry's constant b_1. As shown in Table 2, the isosteric heats of adsorption of propane and ethane on activated carbon are 4.08×10^7 and 3.35×10^7 J/kmol, respectively. Schork and Fair (1988) reported the isosteric heat of adsorption of propane on the same activated carbon to range from about 3.35×10^7 to 4.60×10^7 J/kmol.

The FH-VSM theory implies that the adsorption capacity is independent of temperature and the total number of entities

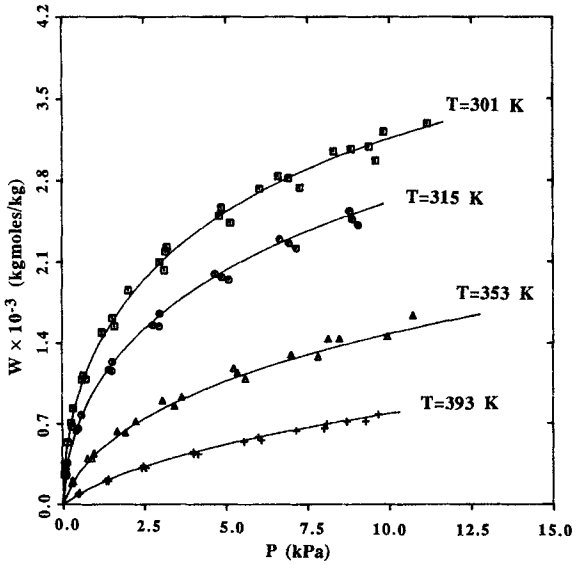

Figure 1. Isotherm data of pure propane on Witco JXC activated carbon.

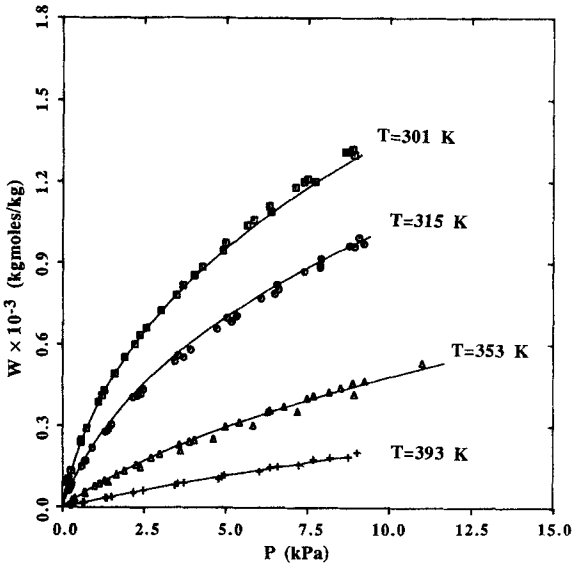

Figure 2. Isotherm data of pure ethane on Witco JXC activated carbon.

(molecules and vacancies) in the vacancy solution does not change with coverage. Therefore, the isosteric heat of adsorption for FH-VSM is independent of surface coverage. The heat of adsorption, however, usually varies with the surface coverage. Recently, Talu and Kabel (1987) pointed out that the experimental heats of adsorption vary by only 10–20% from the constant values obtained by FH-VSM correlations. They concluded that the use of FH-VSM is appropriate for cases where greater rigor is unnecessary.

From experimental data, it can be deduced that propane is more adsorbable on the activated carbon than ethane. The experimental isotherm data are consistent with literature data. Schork and Fair (1988) measured isotherm data of propane on the same Witco carbon. Szepesy and Illés (1963) determined isotherm data of pure propane and ethane as well as their mixtures on Nuxit-AL activated carbon. Even though the adsorbents are different, the isotherms were found to be approximately the same.

Nitrogen and helium at ambient temperature and atmospheric pressure are generally considered inerts on activated carbon. Based on nitrogen isotherm data from Schork (1986), however, nitrogen may be competitive with ethane for adsorption when the partial pressure of nitrogen is much higher than that of ethane. The nitrogen isotherm is reported by a linear isotherm equation (Schork and Fair, 1988) as follows.

$$w_c = 1.30 \times 10^{-9} \exp\left(\frac{1{,}752}{T}\right) P \qquad (6)$$

Based on this isotherm, the heat of adsorption of nitrogen on activated carbon is calculated to be about 1.46×10^7 J/kmol. According to Schork's study, the heat of adsorption of nitrogen should be included in the energy balance. Helium is not adsorbed on nickel silica even up to 1.42×10^4 kPa (Selwood, 1962, p. 179) and not adsorbed on activated charcoal at liquid nitrogen temperature or below (Kirk-Othmer, 1980). It can be assumed that no helium is adsorbed on activated carbon at room

temperature and several atmospheres pressure. Therefore, both mass and heat balances of helium on carbon can be neglected.

Mixture Isotherms Prediction

There are four experimental methods generally used for measuring mixture isotherms: volumetric, gravimetric, manometric, and chromatographic. For whatever method used, direct measurement of multicomponent isotherms is complicated and tedious (Sircar and Myers, 1973). Many researchers have developed techniques for estimating multicomponent adsorption equilibria from pure-component isotherms. These techniques can be classified into four groups. In the first group, the pure-component isotherm equation is simply extended to the multicomponent isotherm equation. This approach has the main advantage of simplicity and is widely used for design purposes, but has two disadvantages: thermodynamic inconsistency and ambiguous constants. Ruthven (1984) suggested using this approach with caution.

The second group of techniques utilizes potential theory. Grant and Manes (1966) successfully applied this theory to predict binary mixture isotherms. A third group, proposed by Ruthven et al. (1973), is known as the general statistical model. This statistical model predicts multicomponent isotherms very well, particularly for zeolite adsorbents.

The fourth group of techniques is developed from thermodynamic solution theories. Based on the assumption of the adsorbed phase activity coefficient, this group can be categorized by two approaches, ideal adsorbed solution theory (IAST) and real adsorbed solution theory (RAST). The IAST was first proposed by Myers and Prausnitz (1965) with the assumption that the adsorbed phase is ideal and therefore the activity coefficient of each component is unity. Five IAST models with different choices of standard states have been reviewed by Sircar and Myers (1973). Myers (1984) concluded that agreement of IAST with experiment is excellent up to about 50% of saturation. The mixture isotherm is specified at constant temperature and spreading pressure. Therefore, the spreading pressures are the same for all components of a mixture. The spreading pressure of each component can be obtained by integrating the pure component isotherm according to the Gibbs equation. However, there is currently no pure component isotherm equation which not only fits experimental data but also permits analytical integration for spreading pressure calculation. O'Brien and Myers (1985) presented a new isotherm equation, which is analytically integrable, and tried to shorten the computation time required for mixture isotherm prediction. Nevertheless, this isotherm equation does not fit well for different gas-solid systems.

For the RAST, Suwanayuen and Danner (1980a, b) first proposed the vacancy solution model (VSM) without the assumption of an ideal adsorbed phase. The activity coefficients are determined by the Wilson (W-) equation. Cochran et al. (1985a, b) introduced the Flory-Huggins (FH-) activity coefficient to improve the VSM approach. Temperature dependency and the interaction between adsorbates are considered in this model. The FH-VSM model has been successfully used to predict mixture isotherms of many adsorbate-adsorbent systems.

Based on the vacancy solution model of adsorption in conjunction with the Flory-Huggins activity coefficient equations, Cochran et al. (1985a) derived the following equation for mixture equilibrium between gas and adsorbed phases.

$$y_i\phi_i P = \gamma_i^s x_i \frac{w_m}{w_m^\infty}\frac{w_i^\infty}{b_i}\left[\frac{\exp\alpha_{iv}}{1+\alpha_{iv}}\right]\exp\left\{\left[\frac{w_i^\infty - w_m^\infty}{w_m} - 1\right]\ln(\gamma_v^s x_v^s)\right\} \tag{7}$$

In Eq. 7, ϕ is a fugacity coefficient which can be set equal to unity for moderate pressures, and γ is an activity coefficient. For binary mixture adsorption, the activity coefficients can be calculated by the Flory-Huggins equations. According to the definition of a vacancy solution, the mole fractions of the adsorbed vacancy solution, x_i^s and x_v^s, are different from the mole fraction of the adsorbed solution, x_i, on a vacancy-free basis.

The FH-VSM model has been tested for a number of adsorption systems by Cochran et al. (1985a, b). Since the present study involved propane-ethane-activated carbon, this particular system was also tested by the present authors. The experimental data of pure component and mixture isotherms are from the publications by Szepesy and Illés (1963a, b, c). The largest deviation between predicted and experimental total amounts of mixture adsorption was only 3.7%. This error is small enough to be acceptable for fixed-bed design purposes. Even though the adsorbent in the present study differed from that used by Szepesy and Illés (1963a, b, c), the pure-component isotherm data are consistent as mentioned above. The FH-VSM appears to be a good method for predicting mixture isotherms, and therefore was chosen for the present study.

Experimental System

The testing system selected in the present study was propane, ethane, helium, nitrogen, and activated carbon. Both adsorbates, propane and ethane, were more than 99.5% pure. The helium was chromatographic grade (99.998%) and the nitrogen was industrial grade (99.6%); these gases were used as carriers and for purging during regeneration. A primary standard calibration gas of 1.00($\pm$0.01) wt. % propane and ethane in nitrogen was used.

Witco JXC activated carbon was used; this petroleum-based carbon was formerly marketed by National Carbon Company as Columbia Type J. Approximately 90% of the total surface area is present in pores of 10 to 25 angstroms. Other physical properties of the adsorbent as measured by Schork (1986) and supplied by the manufacturer are presented in Table 3.

A bench-scale unit was used to study nonisothermal adsorption and hot purge regeneration. A flow diagram of the equipment is shown in Figure 3. Details of construction may be found elsewhere (Huang, 1987). A Union Carbide three-channel gas blending system was used to obtain gas mixtures in the ratios of interest. This system consists of a Readout and Control (ROC) Unit, and a Gas Control Assembly. The latter comprises three Flow Control Modules (FCM), one for each component, for particular flow rate ranges. The outlets of the FCM are manifolded to provide a single outlet for the desired gas mixture. A check valve in the outlet line of each FCM prevents backflow of gas into the module. The percentage of each component is controlled by the ROC Unit, and actual flow through each channel is displayed digitally. Flowmeters of the gas blender system were factory-calibrated for nitrogen, propane and ethane for three channels. A correction factor for helium was provided. The composition of the exit gas mixture from the gas blender could be calculated from the flow rates and was checked by gas chromatography. The deviations were within 6.9%.

Table 3. Physical Properties of Witco JXC 8 × 10 Activated Carbon

	Manufacturer's Data	Experimental Data
Surface area (m^2/kg)	1.10×10^6	1.16×10^6
Bulk density (kg/m^3 bed)	4.81×10^3 (max.)	4.61×10^3
Specific heat (J/kg · K)	8.37×10^2 (367 K) 1.17×10^3 (700 K)	—
Geometric surface area a_p (m^{-1})		2.41×10^3
Equivalent radius R_{p1} (m)		1.6×10^{-1}
Equivalent radius R_{p2} (m)		1.2×10^{-1}
Porosity ϵ_p		0.60
Bed void fraction ϵ_{ex}		0.44

A Varian 3700 Gas Chromatograph with two flame ionization detectors (FID's) was used to analyze the bed effluents. Two Chromosorb 101 packed columns were used to separate the effluent samples. The longest retention time of the chromatographs under conditions of interest was less than 4 minutes. In order to get more data points, the two FID's and the two columns were used alternately. Effluent samples were taken and injected every two minutes by a Valco 10-port multifunctional gas sampling valve with a two position electric valve actuator. A Varian 4270 integrator was used to record the chromatographs, report the results, and control the Valco sampling valve injection.

The adsorption vessel was fabricated from stainless steel and was 33 cm long with a 30.5 cm packed section, 7.62 cm outside diameter and 0.089 cm thick walls. Four thermocouples were located in the bed 10 and 20 cm from the top of the packed section, at the center and at half the bed radius. Two thermocouples were installed above and below the column. These thermocouples were exposed-tip, type J, in 0.16 cm sheaths. Four surface thermocouples were attached to the outside of the bed at each quarter height of the packed section. All the thermocouples were connected to an Omega 2700A digital thermometer through a relay system controlled by a TRS Color Computer 2. A data acquisition system allowed all thermocouples to be read within five seconds. Temperatures were recorded each 15 seconds.

A complete discussion of system design and operating procedure can be found elsewhere (Huang, 1987).

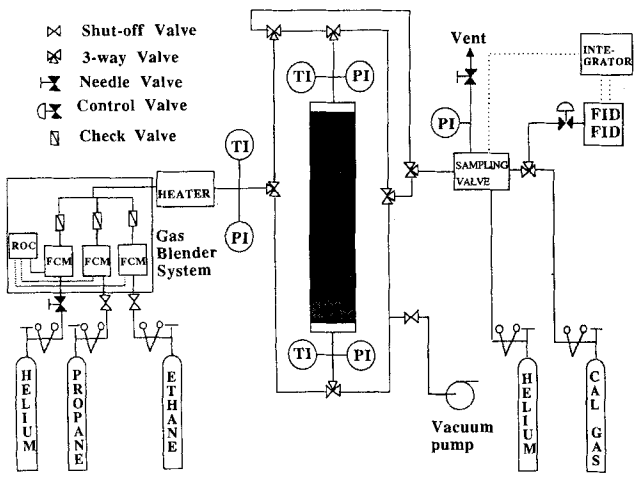

Figure 3. Flow diagram of experimental equipment.

Dynamic Model Development

Mass transfer mechanism

In general, the mass transfer mechanism of an adsorption process includes four steps: fluid-film transfer, pore diffusion, surface adhesion, and surface diffusion. Since the surface adhesion rate approximates the order of the collision frequency of the gas on the solid surface, which is much greater than for the transport processes, equilibrium is assumed to be reached instantaneously at the interfaces (Yang, 1987). Adsorbates initially transfer from the bulk gas through an external film and to the external surface of the particles. Molecules of the adsorbates diffuse into the pores of the particle, are adsorbed on the active sites, and then diffuse along the surface. Film transfer and pore diffusion are treated as sequential steps, but pore diffusion and surface diffusion generally take place in parallel. Any combination of the resulting three steps can constitute the rate-controlling mechanism. The mechanism may vary with adsorbate-adsorbent system and operating conditions.

The external film mass transfer resistance is determined by the hydrodynamic conditions. It is convenient to represent mass transfer rate in terms of an effective transfer coefficient (k_{fi}) as a linear driving force equation.

$$N_{fi} = -k_{fi}(c_{bi} - c_{sur,i}) \tag{8}$$

There are several empirical correlations for the film transfer coefficient available in the literature. For the low Reynolds number region covered in the present study, the widely-used correlation of Petrovic and Thodos (1968) was adopted:

$$k_{fi} = \frac{0.357}{\epsilon_{ex}} (N_{Re})^{0.64} (N_{Sc})^{0.33} \frac{D_{im}}{2R_p}, \quad 3 < N_{Re} < 2{,}000 \tag{9}$$

An analogy to this equation was used to calculate the heat transfer coefficient. The Petrovic/Thodos correlation was developed for spherical particles, and is used here for cylindrical pellets by replacing R_p with the radius of a sphere of equivalent external surface area. In the following discussion, we assume that mass transfer within cylindrical particles can be approximated by mass transfer within a sphere of equivalent radius.

The molecular diffusion of a component in a mixture is generally complicated, as described by the Stefan-Maxwell equation. For single-component diffusion in a mixture, however, the diffusion coefficient D_{im} for the component is approximately related to the binary coefficients by the following relationship (Wilke, 1950):

$$D_{im} = \frac{1 - y_i}{\sum_{\substack{j=1 \\ j \neq i}}^{n} \frac{y_j}{D_{ij}}} \tag{10}$$

When the diffusing components are present in low concentration, as in the present study, the substitution of D_{im} from Eq. 10

into equations for single-component diffusion should introduce no great error (Satterfield, 1981). The mutual diffusion coefficient in a low-pressure binary gas mixture can be calculated from the Chapman-Enskog formula (Bird et al., 1960).

In porous solids, pore diffusion may occur by ordinary and Knudsen diffusion. For our temperature and pressure ranges, the mean free paths of propane and ethane are greater than 125 and 225 Å, respectively. According to the manufacturer, JXC carbon has only about 3% of the total pore volume in which the pore diameter is larger than 100 Å. One would thus conclude that Knudsen diffusion contributes more significantly to the flux through the pores than does ordinary diffusion and that the contribution of ordinary diffusion is negligible.

The Knudsen diffusion coefficient can be estimated by (Satterfield, 1980):

$$D_{ki} = 9.7 \times 10^{-5} \frac{r_e}{\tau_p} \left(\frac{T}{M_i}\right)^{0.5} \tag{11}$$

Approximated as $2\epsilon_p/(S\rho_p)$, the mean pore diameter (r_e) is about 12 Å for JXC carbon. The pore tortuosity factor (τ_p) is approximately set at 4.0 (Satterfield, 1980). Knudsen diffusion coefficients of propane and ethane at 21°C calculated by Eq. 11 are 7.5×10^{-8} and 9.1×10^{-8} m^2/s, respectively. Costa et al. (1985) reported the internal diffusion coefficient of ethane on AC-40 activated carbon to be 1.0×10^{-8} m^2/s at 20°C, which compares well with the value calculated here.

By analogy to Fick's law, a surface diffusion coefficient (D_s) may be defined in terms of a surface concentration (C_s) or of an adsorbed phase concentration (w_i) as in the following equation (Smith, 1981):

$$N_{si} = -D_{si} \frac{dC_{si}}{dr} = -D_{si}\rho_p \frac{dw_i}{dr} \tag{12}$$

The surface diffusion is an activated process which can be expressed by an Arrhenius-type expression (Smith, 1981):

$$D_{si} = D_{so,i} \exp\left(\frac{-E_{si}}{RT}\right) \tag{13}$$

where E_{si} is the activation energy for surface diffusion. Based on their correlation of literature data, Sladek et al. (1974) proposed that the activation energy be approximated as 45% of the heat of physical adsorption for nonpolar adsorbates. They also suggested that D_{so} be estimated as follows:

$$D_{so} = \frac{1.61 \times 10^{-6}}{\tau_s} \tag{14}$$

The surface tortuosity factor τ_s is often assumed equal to τ_p in the absence of a better approximation (Satterfield, 1981).

Schneider and Smith (1968) reported values of 5.5×10^{-9} and 1.5×10^{-9} m^2/s for the surface diffusivities of ethane and propane, respectively, on silica gel at 323 K. Costa et al. (1985) reported an average value of 3.8×10^{-10} m^2/s for ethane on AC-40 activated carbon at 293 K. Based on Eqs. 13 and 14, and the given heats of adsorption, the surface diffusion coefficients of ethane and propane on JXC carbon at 294 K are 8.6×10^{-10} and 2.2×10^{-10} m^2/s, respectively. Although the adsorbents are different, the values are in agreement.

As mentioned earlier, surface adhesion is essentially instantaneous. A local equilibrium can be assumed between the gas phase in the pore and the solid phase. Since pore diffusion and surface diffusion take place in parallel, the total flux at the pore mouth of the particle surface is:

$$N_{fi}|_{r=R_p} = -D_{ki} \frac{\partial c_i}{\partial r}\bigg|_{r=R_p} - D_{si} r_p \frac{\partial w_i}{\partial r}\bigg|_{r=R_p} \tag{15}$$

The solid-phase concentration inside the pore (w_i) is a function of temperature and the gas phase composition. Because heat transfer is rapid, the temperature can be assumed uniform inside the particle. Therefore, Eq. 15 can be rewritten in the following manner:

$$N_{fi}|_{r=R_p} = -D_{ki} \frac{\partial c_i}{\partial r}\bigg|_{r=R_p} - D_{si}\rho_p \sum_{j=1}^{n} \left(\frac{\partial w_i}{\partial c_j}\right) \frac{\partial c_j}{\partial r}\bigg|_{r=R_p} \tag{16}$$

In the present study, the adsorbate concentrations are dilute. The solid-phase concentration of each adsorbate may be assumed to be independent of the gas-phase concentration of the other adsorbate. In other words, the total flux of the ith component at the pore mouth of the particle is

$$N_{fi}|_{r=R_p} = -D_{ki} \frac{\partial c_i}{\partial r}\bigg|_{r=R_p} - D_{si}\rho_p \left(\frac{\partial w_i}{\partial c_i}\right) \frac{\partial c_i}{\partial r}\bigg|_{r=R_p} \tag{17a}$$

or

$$N_{fi}|_{r=R_p} = -D_{pe,i} \frac{\partial c_i}{\partial r}\bigg|_{r=R_p} \tag{17b}$$

where

$$D_{pe,i} = D_{ki} + D_{si}\rho_p \frac{\partial w_i}{\partial c_i} \tag{18}$$

From Eqs. 8 and 17, an effective overall mass transfer coefficient can be defined.

$$N_{fi} = -K_{eff,i}\,(c_{bi} - \bar{c}_i^*) \tag{19}$$

where

$$\frac{1}{K_{eff,i}} = \frac{1}{k_{fi}} + \frac{(c_{sur,i} - \bar{c}_i^*)}{D_{pe,i}\left(\frac{\partial c_i}{\partial r}\right)} \tag{20}$$

The gas-phase concentration profile within the particle is assumed to be parabolic (Tsai et al., 1983):

$$c_{ip} = c_0 + c_2 r^2 \tag{21}$$

For a sphere of radius R_p, the average gas-phase concentration $\bar{c}_{ip}$ is then defined by

$$\bar{c}_{ip} = 3 \int_0^1 R^2 c_{ip}\, dR \tag{22}$$

where $R = r/R_p$. By substituting Eqs. 21 and 22 into Eq. 20, the effective overall mass transfer coefficient is then derived as follows:

$$\frac{1}{K_{eff,i}} = \frac{1}{k_{fi}} + \frac{R_p}{5\,D_{pe,i}} \tag{23}$$

Note that $K_{eff,i}$ is the same as that derived by Glueckauf (1955) for systems with favorable isotherms and constant intraparticle diffusivities.

Mathematical modeling

For developing a dynamic model of a fixed-bed adsorber, sets of mass and energy balances must be considered: component mass balance within the gas phase and the solid phase; and the energy balance around the gas phase, the solid phase, and column wall. The major assumptions made in the development are that:

1. The system pressure is constant.
2. The gas phase is dilute and follows ideal gas behavior.
3. The carrier gas flow rate is constant.
4. Radial velocity, temperature, and concentration gradients within the bed are negligible.
5. Accumulation of carrier gas or adsorbates in the pores of the solid phase is negligible.
6. Axial conduction within the column wall is negligible.
7. The heat capacity of the gas within the pores of the solid phase is negligible relative to that of the solid.
8. The amount of carrier gas adsorbed is negligible.
9. The cylindrical adsorbent pellets can be modeled as spheres.
10. All transport coefficients are independent of concentration.
11. Mutual interactions are taken into account only through the isotherm equation.
12. The temperature within the particle is uniform.

Applying the above assumptions to the component balance of the gas phase through a packed bed, the following equation is obtained.

$$\frac{\partial y_i}{\partial t} = \frac{-G}{c\epsilon_{ex}}\frac{\partial y_i}{\partial z} + D_{Li}\frac{\partial^2 y_i}{\partial z^2} - \frac{\alpha_p(1-\epsilon_{ex})}{\epsilon_{ex}} K_{eff,i}(y_i - y_i^*) \tag{24}$$

The component balance within the solid phase is simply stated as

$$\frac{\partial w_i}{\partial t} = \frac{\alpha_p(1-\epsilon_{ex})}{P_s} K_{eff,i} c\,(y_i - y_i^*) \tag{25}$$

The energy balance around the gas phase in the packed bed includes heat transfer to the solid phase and to the column wall, as well as axial conduction:

$$\frac{\partial T_g}{\partial t} = \frac{-G}{c\epsilon_{ex}}\frac{\partial T_g}{\partial z} + \frac{k_{ax}}{cc_{pg}}\frac{\partial^2 T_g}{\partial z^2} - \frac{h_f \alpha_p(1-\epsilon_{ex})}{\epsilon_{ex} c c_{pg}}(T_g - T_s) - \frac{2h_w(T_g - T_c)}{R_b \epsilon_{ex} c c_{pg}} \tag{26}$$

The energy balance around the solid phase includes the heat generated by sorption of adsorbates and carrier gas. If the carrier gas is helium, there is no heat of adsorption of carrier gas.

$$\frac{\partial T_s}{\partial t} = \frac{\alpha_p(1-\epsilon_{ex})}{\rho_s} \cdot \left[\frac{h_f(T_g - T_s) + \Sigma\,\Delta H^i_{ads}\, c\, K_{eff,i}(y_i - y_i^*)}{c_{ps} - (\Delta H_c)\left(\frac{\partial w_c}{\partial T_s}\right)}\right] \tag{27}$$

Heat transfer from the gas phase and to the atmosphere is included in the energy balance around the column wall.

$$\frac{\partial T_c}{\partial t} = \frac{h_w \alpha_c}{\rho_c c_{pc}}(T_g - T_c) - U_{ins}\frac{\alpha_i}{\rho_c c_{pc}}(T_c - T_{amb}) \tag{28}$$

The associated initial conditions are as follows, for $0 < z < L$:

$$w_i(0, z) = w_{i,0}(z); \quad c_i(0, z) = c_{i,0}(z);$$
$$T_g(0, z) = T_{g,0}(z); \quad T_s(0, z) = T_{s,0}(z);$$
$$T_c(0, z) = T_{c,0}(z)$$

The initial gas- and solid-phase concentrations for the adsorption step are zero. For the regeneration step, they are the values of final conditions of the previous adsorption step. Boundary conditions at $z = 0$ and $z = L$ and for $t > 0$ are:

$$c_i(t, 0) = c_{i,in}(t); \quad T_g(t, 0) = T_{gin}(t);$$
$$\frac{\partial c_i(t, L)}{\partial z} = 0; \quad \frac{\partial T_g(t, L)}{\partial z} = 0$$

The quantities $c_{i,in}$ and T_{gin} may be functions of time. However, they are maintained constant in the present study. For the regeneration step, $c_{i,in}$ is zero.

At the low concentrations considered in our study, the physical properties of the gas phase are assumed to be those of the carrier or purge gas. These properties are calculated as functions of temperature. The physical properties of the adsorbent and the column wall are considered constant.

End effects in experimental equipment

As indicated earlier, there are 1.27 cm high spaces before and after the packing section. These spaces represent significant heat sinks and the energy balances around them must be considered. At the inlet, the temperature of the gas entering the packed bed, $T_{gi,n}$, is calculated given the temperature of the gas entering the inlet section, T_{g0}. Similarly, the temperature of the gas exiting the column, $T_{g,out}$ is calculated, given the temperature of the gas at the bed exit, T_{gL}.

The inlet and outlet sections of the column are modeled as continuous stirred tanks. The corresponding equations for this are:

$$\frac{dT_c}{dt} = \frac{(h_w A)}{c_{pc} m}(T_{g2} - T_c) - \frac{(UA)}{c_{pc} m}(T_c - T_{amb}) \tag{29}$$

$$\frac{dT_{g2}}{dt} = \frac{G\pi R_b^2}{cV}(T_{g1} - T_{g2}) - \frac{(h_w A)}{cVc_{pg}}(T_{g2} - T_c) \tag{30}$$

where Tc refers to the temperature of the column wall in the inlet or outlet section, T_{g1} is the temperature of the gas entering the section, and T_{g2} is the temperature of the exit gas from the section.

Numerical technique

For a process with two adsorbates, there are seven partial differential equations (PDE) for energy and mass balances within the packed bed. The mass flux into the solid particles is represented by a linear driving force model with a variable lumped-resistances transfer coefficient. The overall transfer coefficient $K_{eff,i}$ is calculated from Eq. 23. The interfacial equilibrium concentration, y_i^*, is calculated from the FH-VSM (Eq. 7). The PDE's representing the packed bed were solved by the numerical method of lines (NMOL). The spatial dimension was discretized using second-order central differencing. The resulting set of ODE's was solved using DGEAR. (This program employs Gear's method with variable order and step size.) The Neumann boundary conditions were represented by second-order backwards differencing at $z = L$. The number of axial grid nodes used was at least 24 for a 30 cm long bed.

Two main frame computer systems, CDC Dual Cyber 170/750A and Cray X-MP/24, were used to solve the complicated mathematical problem. The typical computation time of a complete adsorption-regeneration cycle run on the CDC computer was about 10 minutes; on the Cray supercomputer the same cycle took about 80 seconds.

Results and Discussion

Inert gas heating simulation

Based on the energy balance equations discussed above, there are five adjustable variables: U_{ins}, h_w, $(UA)_T$, $(UA)_B$, and (h_wA). Schork (1986) found that the set of values in Table 4 provided reasonable fits to six sets of measured nitrogen heating data.

Since the adsorption column and the adsorbent used in this study were the same as used by Schork, the values of heat transfer coefficients could be used to simulate the inert gas heating data for both nitrogen and helium. For confirmation, one additional nitrogen plus two helium heating runs were made in the present study. Typical experimental data and modeling results for helium heating are compared in Figure 4. Since the comparisons are good, all heat transfer coefficients were retained for use in the adsorption and regeneration simulations. It should be mentioned that the temperature data for the bed exit are unreliable since that particular thermocouple was found to be unstable.

Dynamic experimental results

Nineteen adsorption and regeneration cycle runs were made. The operating conditions are summarized in Table 5. The run

Table 4. Heat Transfer Coefficients

$U_{ins} = 2.01$ W/m^2 · K
$(UA)_T = 3.138 \times 10^{-3}$ W/K
$(UA)_B = 1.883 \times 10^{-2}$ W/K
$h_w = 3.43 \times 10$ W/m^2 · K
$(h_wA) = 1.255$ W/K

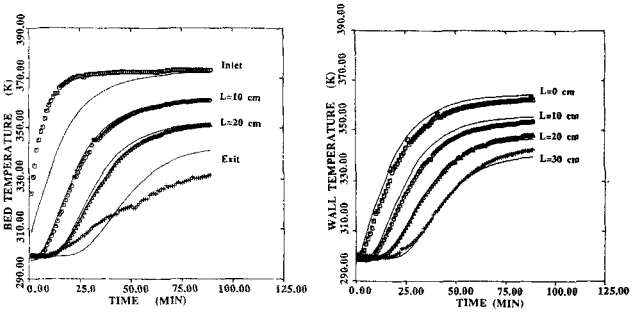

Figure 4. Bed and wall temperatures for heating a clean bed with hot helium.

numbers of adsorption and regeneration correspond to each other, except for Run 27. The 27th run was a cyclic run which consisted of sequential steps of adsorption (AD-271, 272, and 273) and regeneration (DE-27). The gas flow rates employed, 3.53×10^{-3} to 7.32×10^{-3} kmol/m^2 · s, span the range of typical industrial operations. The propane and/or ethane concentration of the inlet gas stream for adsorption runs ranged from 0 to 1.5 mol %. The temperature of the inlet gas for the adsorption runs was approximately room temperature. The temperature of the purge gas was limited at the upper end by the heater capacities. The system pressure was maintained at either 170 or 239 kPa. The direction of gas flow for regeneration was countercurrent to the adsorption direction. The gas flow was upward during adsorption except for Runs AD-3, AD-4, and AD-22. The bed was taken to full saturation in all adsorption runs except AD-21, which was halted at breakthrough. Both carrier gas and purge gas in a particular cycle run were the same, either helium or nitrogen.

The adsorption capacity of the bed is presented in Table 6. The equilibrium bed capacities were based on pure component saturation at the inlet temperature of each run. The actual quantities during adsorption were determined by calculating the differences between the total amount of input adsorption and the output during the desorption step. The lowest relative capacity of propane is 94%. However, the adsorption capacity of ethane in the binary mixture ranged from 12 to 36% of its single component equilibrium value. Clearly, propane is more strongly adsorbed than ethane. The nonkey component (ethane) moves more quickly than the key component (propane) and is adsorbed on the fresh carbon downstream of the bed. The nonkey component is displaced or purged out from the adsorbent while the key component is being adsorbed in its place. After complete breakthrough of the key component, only a small fraction of the nonkey component is left in the bed. For single-component adsorption runs (except Run AD-17) the actual bed capacities are approximately equal to their predictive equilibrium capacities. There is only 79% of relative capacity for Run AD-17. The reason for this anomaly may be that the carrier gas (nitrogen) competes with ethane for adsorption.

The stoichiometric breakthrough time t_s is also provided in Table 6. All of these times were predicted under the assumption of pure component isothermal adsorption at the inlet temperature. Evidently, the stoichiometric breakthrough time of propane is much longer than that of ethane.

Examples of the effluent temperature and concentration data and the temperature data inside the bed for a typical adsorption-regeneration cycle run (AD/DE-14) are presented in Figures 5

Table 5. Operating Condition of Adsorption Runs

Run No.	Y_{c3in}	Y_{c2in}	Adsorption step $G \times 10^{-3}$	Inert	T_{inlet}	P	Regeneration step $G \times 10^{-3}$	Purge	T_{reg}	P
8	1.50	0.72	5.28	He	295.6	170	5.16	He	360.4	170
14	0.70	0.73	5.21	He	295.2	239	5.14	He	368.2	239
17	0.0	0.73	5.17	N_2	295.8	239	5.12	N_2	375.4	239
21*	0.71	0.75	5.21	N_2	296.4	239	5.14	N_2	376.0	239
22**	0.71	0.73	5.21	N_2	294.8	239	5.14	N_2	375.4	239
26	0.70	0.0	5.20	He	296.1	239	5.16	He	372.1	239
271	0.0	0.74	5.17	He	295.8	239	5.14	He	374.9	239
272	0.72	0.0	5.17	He	295.8	239				
273	0.0	0.73	5.17	He	295.8	239				

*Downward run for adsorption step
**Partial saturation run
y, mol %
G, kmol/m^2 · s
T, K
P, kPa

and 6, respectively. The breakthrough curve of the key component (propane) is still sigmoid, as in the case of pure component adsorption. However, the breakthrough curve of the nonkey component (ethane) is totally different from that of the pure-component adsorption process. The effluent concentration of ethane rises very rapidly after it breaks through, and overshoots its inlet composition. This "roll-up" phenomenon of the nonkey component during adsorption is clearly shown in Figure 5. The effluent concentration of ethane then decreases to its inlet concentration when propane elutes.

Stoichiometric breakthrough times of propane and ethane based on single component prediction are also presented in Figure 5. For single-component adsorption processes, a stoichiometric breakthrough time could be defined as the time when the effluent concentration of the adsorbate reaches half of its inlet concentration. However, for multisolutes adsorption processes, the breakthrough curve of the key component shifts to the left because part of the adsorbent active sites may be occupied by the nonkey component molecules. The nonkey component breaks through much earlier than its stoichiometric time, based on pure component prediction. This is because of the preferential and competitive adsorption of the key component.

After the bed was saturated with adsorbates, the regeneration process was started by using hot purge gas. The ordinate of Figure 6 is the ratio of effluent concentrations of the regeneration run to inlet concentrations of the corresponding previous adsorption run. Hereafter, all figures of depletion curves are presented in this same manner.

As mentioned earlier in this section, only a fraction of the ethane is left in the bed after complete breakthrough of propane. Accordingly, the depletion curves of ethane drop rapidly, because of rapid purging. Conversely, since most of the bed is saturated with propane, the regeneration time for propane is much longer. As shown in Figure 6, the effluent concentration of propane may rise above its initial concentration in the bed, similar in nature to roll-up during adsorption. The roll-up of the propane depletion curve may not occur when the regeneration temperature is below a certain value. Nevertheless, the depletion curve of propane for the thermal regeneration process will always have a local maximum. This is because the propane molecules desorbed from the upstream section of the bed readsorb and accumulate in the cooler downstream section. For lower regeneration temperatures, the amount of propane accumulated in the downstream end of the bed is not high enough to cause overshoot of its initial concentration.

The other important feature of the propane depletion curve is the existence of the dip in the first few minutes of the regeneration process. This can be seen clearly in Figure 6. As the hot purge gas initially enters the cool bed, it removes adsorbates from the bed void volume and is cooled by the cold bed. There is a driving force between purge gas phase and adsorbed phase to diffuse the adsorbates out. Since the desorption process is endothermic, the temperature of purge gas at a downstream point may drop below the initial bed temperature or the ambient temperature. Furthermore, because heat transfer is more rapid than mass transfer, the downstream portion of the bed is

Table 6. Adsorption Capacity of the Bed

Run No.	Equilibrium Capacity* Ethane	Equilibrium Capacity* Propane	Actual Adsorption* Ethane	Actual Adsorption* Propane	Percentage (%) Ethane	Percentage (%) Propane	Stoichiometric Breakthrough Time** Ethane	Stoichiometric Breakthrough Time** Propane
8	0.2976	1.339	0.0455	1.309	15.0	98.0	30.0	64.8
14	0.3744	1.146	0.0918	1.134	25.0	99.0	37.6	119.6
17	0.3685	—	0.2928	—	79.0	—	37.4	—
21	0.3695	1.126	0.1124	0.922	30.0	82.0	36.0	115.9
22	0.3772	1.160	0.0985	1.101	26.0	95.0	38.2	119.9
26	—	1.127	—	1.155	—	102	—	117.9

*mkmol
**minutes

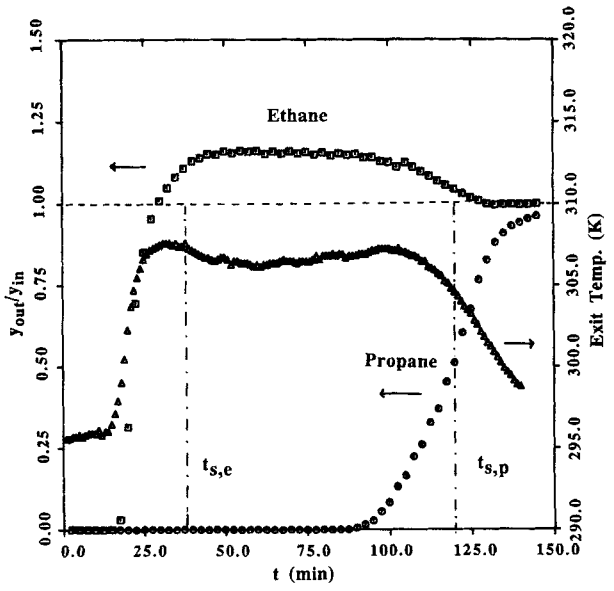

Figure 5. Typical experiment breakthrough data (Run AD-14).
Stoichiometric breakthrough times are denoted as $t_{s,e}$ and $t_{s,p}$.

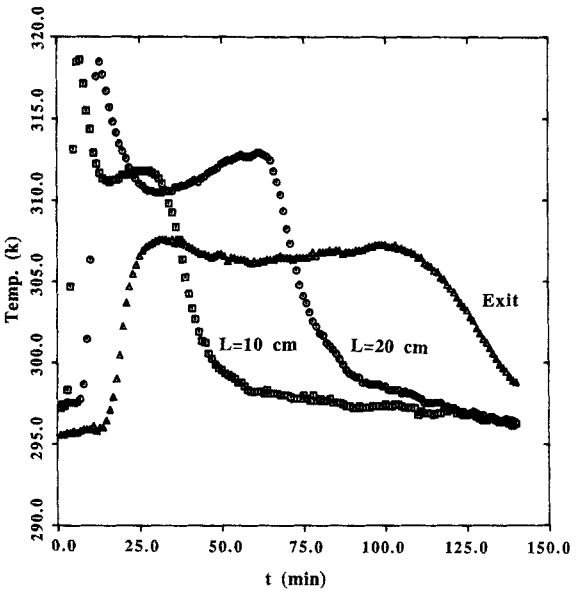

Figure 7. Temperature histories during adsorption, at different points inside the bed, $r = 0.5R_b$ (Run AD-14).

exposed to a relatively cool purge gas. This causes the bed temperature to drop and the driving force for readsorption to increase. Because the propane in the bed void volume is removed very quickly and the propane molecules purged upstream are readsorbed on downstream sites, the effluent concentration of propane drops to a certain value. This causes the dip of the propane depletion curve.

Typical temperature data measured at different heights of the bed (10 and 20 cm from entrance for $r = \frac{1}{2} R_b$, and exit) during the adsorption and regeneration steps are shown in Figures 7 and 8, respectively. The temperature curves demonstrate the importance of heats of adsorption in the gas adsorption process. Even with relatively low feed concentrations (about 0.7 mol % for both ethane and propane) there were significant rises of system temperature. As shown in the figures, the system temperature 10 cm from the entrance rose sharply due to the heat released by both adsorption of ethane and propane on the activated carbon. Because of the displacement of ethane by propane, the system temperature could keep changing or remain constant. For the case of low propane feed concentration, the heat released by propane adsorption is offset by energy required for ethane desorption. As shown in Figure 7, the system temperature then dropped until the energy demand was balanced with the energy supply, after which a temperature plateau was

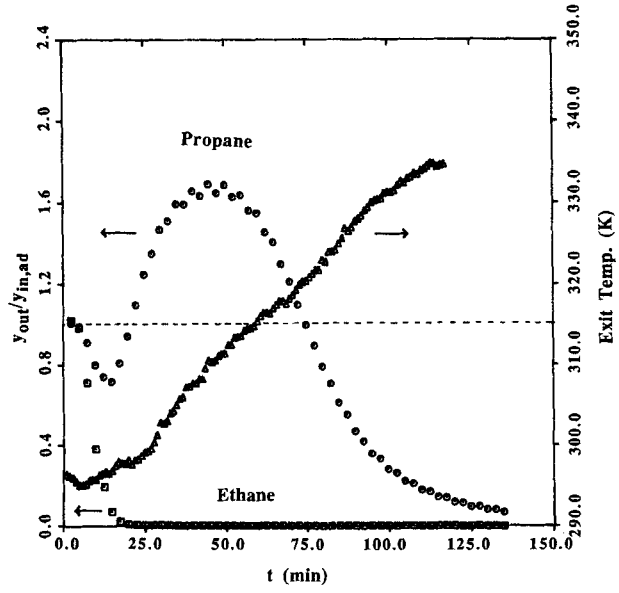

Figure 6. Typical experimental depletion data (Run DE-14).

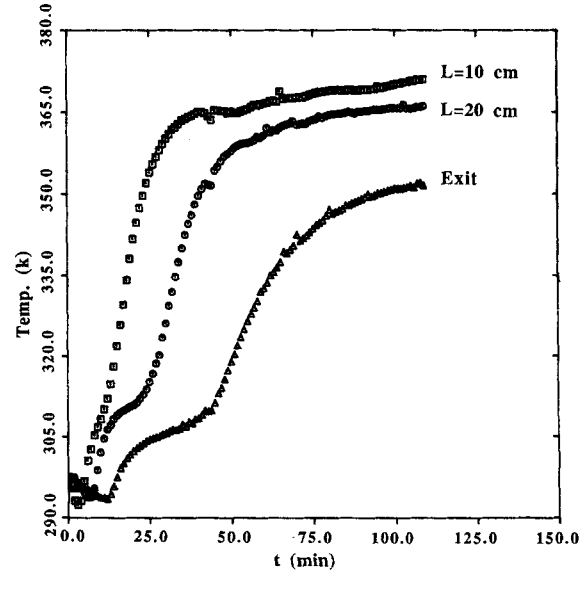

Figure 8. Temperature histories during regeneration, at different points inside the bed, $r = 0.5R_b$ (Run DE-22).

formed. On the other hand, for high propane feed concentration, the system temperature continued to increase. However, the slope of the temperature curve decreased because of ethane desorption. Figure 7 shows that temperature increases at the exit were not as prominent as those inside of the bed. This illustrates the significance of heat losses at the outlet section.

Run 27 is a cyclic process which consists of a sequence of adsorption with intermediate regeneration. The effluent concentration histories of adsorption and regeneration steps of this run are presented in Figures 9 and 10, respectively. In the first phase, the feed gas contained only one adsorbate, ethane, in helium. This was a simple single component adsorption process, and the ethane breakthrough curve had the expected S-shape. After complete breakthrough of ethane, the second-phase adsorption was begun. Propane carried by helium at the same level of inlet concentration and temperature as in the first phase was fed into the bed in the same direction. The adsorbed ethane was purged out by the propane. The depletion curve of ethane is shown to be elongated and unstable. Before the breakthrough of propane, most of the ethane was purged from the bed. Therefore, the last part of the second phase was similar to a single component adsorption and the breakthrough curve of propane was also S-shaped.

In the third phase, the same feed stream as in the first phase (i.e., ethane/helium) was used. Since the bed was saturated with propane at the end of the second phase, only a few sites on the adsorbent were still available for ethane. Hence, ethane broke through very quickly. Because ethane is less strongly adsorbed than propane, only a small amount of propane adsorbed in the bed could be displaced by the ethane. The breakthrough curve of ethane increased asymptotically to 90% of its inlet concentration. Simultaneously, the depletion curve of propane dropped asymptotically to 60% of the propane inlet concentration during the second phase. Eventually, the propane content of the effluent would have dropped to zero. The propane appears suitable for desorbing ethane, but the reverse may not be true.

For regeneration Run 27, hot helium entered the bed countercurrently to the adsorption direction. The ethane depletion curve was as expected, but the propane depletion curve was not. At the end of the third phase of adsorption runs, no propane was left in the bed void volume (interstices between particles). Some of the adsorbed propane was pulled out at the upstream section which

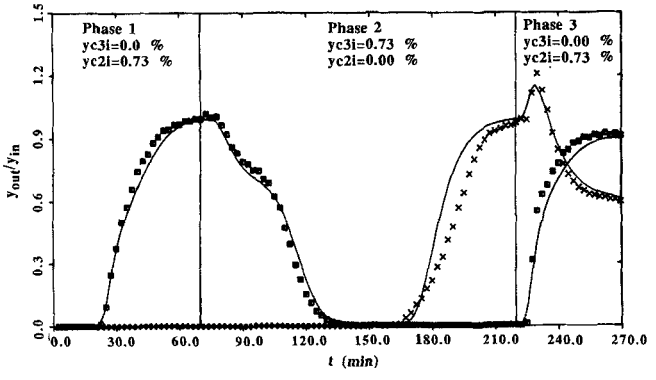

Figure 9. Data and simulation for experimental Run AD-27.

For phase 1, only ethane is adsorbed. For phase 2, the bed saturated with ethane is used to adsorb propane. For phase 3, the bed saturated with propane (from phase 2) is used to adsorb ethane.

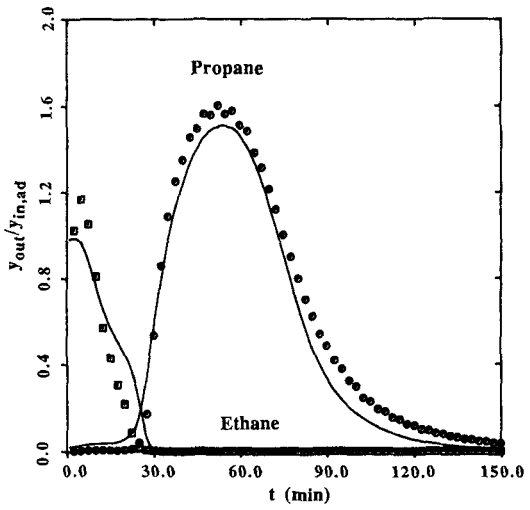

Figure 10. Data and simulation for experimental Run DE-27.

The bed from phase 3 of Figure 9 is regenerated from hot helium.

was the downstream section of the regeneration run. These evacuated sites could readsorb propane molecules at the first stage of regeneration. Therefore, the effluent contained very little propane for the first few minutes of the regeneration run. But when the bed was heated up to a certain temperature, the propane was purged out and its depletion curve showed roll-up as for other regeneration processes.

Adsorption and regeneration simulation

The complete dynamic model described earlier was used to simulate the experimental adsorption and regeneration data. The heat transfer coefficients calculated by simulating inert gas heating data were employed in the simulations of both adsorption and regeneration experiments. A lump-resistances linear driving force model was assumed for calculating the rate of mass transfer. All transport properties were predicted using available correlations.

Schork and Fair (1988) found that variations of axial diffusion and axial thermal conductivity have no effect on either the breakthrough or depletion curves. However, the required computation time increased up to four times when the axial diffusivity was set equal to zero. Therefore, axial diffusion and axial thermal conductivity are retained in the model. The correlation of Edwards and Richardson (1968) was used to calculate the axial diffusion coefficients and the effective axial thermal conductivity.

For modeling a multicomponent adsorption process with a linear driving force model, the lumped-resistances mass transfer coefficients are generally treated as constants (Harwell et al., 1980; Wong and Niedzwiecki, 1982). The primary disadvantage of this assumption is that new values for the mass transfer coefficients must be determined for each run. In addition, there is no empirical correlation available for predicting the overall mass transfer coefficient for an adsorption process. This problem was eliminated by using calculated variable lumped-resistances transfer coefficients.

If all of the component diffusion coefficients and film mass transfer coefficients were known, the lumped-resistances trans-

fer coefficients could be calculated independently of the experimental dynamic data. Unfortunately, the most important coefficient in the adsorption process, surface diffusivity, is the least well known. To estimate surface diffusivity D_s, Eq. 13 was employed in this study. The pre-exponential factor D_{so} is the only adjustable parameter for determining overall mass transfer coefficients. The remaining diffusivities and transfer coefficients were estimated by the appropriate correlations. For the best fit, the values of D_{so} for propane and ethane are 7.7×10^{-7} and 3.1×10^{-7} m^2/s, respectively. These values were used for all simulation runs. Based on these best-fit values of D_{so} plus Eq. 14, the surface tortuosity factor τ_s could be back calculated. The factor ranged from 2.1 to 5.2, which is in reasonable agreement with the value suggested by Satterfield (1981).

As discussed before, the mass transfer mechanism includes internal and external transport processes. The relative importance of internal and external mass transfer resistances may be determined by the Biot number. A high Biot number would indicate that the major resistance is within the pellet. Aris (1975) estimated that the mass Biot number for a packed bed is in the range of 5 to 500. In the present study, the mass Biot number was 1 to 66. Therefore, the intraparticle resistance is more important than the external film resistance in determining the mass transfer rate.

Internal transport involves the parallel processes of gas diffusion in pores and surface diffusion on the pore walls. All adsorbents possess high surface areas, and essentially the entire surface is inside the particle. This high surface area provides a chance for high surface concentration, and thus the surface diffusion dominates the flux in the pores. Costa et al. (1985) observed that the contribution of surface diffusion to the global mass transfer inside the activated carbon could be as much as 70–80% for methane, ethane, and ethylene at 293 K and pressures below 40 kPa.

Because of experimental difficulties in measuring surface diffusivity, it is convenient to lump surface diffusion into an effective diffusivity (Yang, 1987). In the present study, a linear driving force model is used. The effective intraparticle diffusivity is calculated by Eq. 18. The Knudsen diffusion coefficient, D_{ki}, is directly proportional to the square root of the absolute temperature. In a small range of operating temperatures as encountered in the present study, the Knudsen diffusivity can be treated as constant. The surface diffusivity can then be estimated by Eq. 13. The best fit surface diffusivities of propane and ethane on the surface of activated carbon at 294 K are 4.26×10^{-10} and 6.61×10^{-10} m^2/s, respectively. These values of surface diffusivities agree well with those published by Costa et al. (1985). It should be noted, however, that surface diffusivity is strongly dependent on surface coverage, and its local value can vary easily by an order of magnitude.

The influence of surface diffusivity on the breakthrough and depletion curves is presented in Figures 11 and 12. Note that the surface diffusivity is proportional to the pre-exponential factor, D_{so}. Both breakthrough and depletion curves become much sharper as D_{so} increases. As shown in Figure 11, all breakthrough curves of propane (key component) intersect at a point near 55% of its entrance concentration. This feature is similar to that in the single component adsorption case reported by Collins and Chao (1973). The breakthrough curves of ethane (nonkey), however, intersect at a point higher than 60% of its entering concentration. From Figure 12 it may be seen that all depletion curves of ethane intersect at near one-half of its entrance concentration in the previous adsorption step. All depletion curves of propane intersect at a point near its entrance concentration in the previous adsorption step.

For higher values of the surface diffusivity, the mass transfer rates inside the particle are higher, leading to narrower mass transfer zones, if surface diffusion dominates the total flux. Conversely, lower values of D_{so} widen the mass transfer zones. From Figure 11, the breakthrough curves are clearly flatter when the values of D_{so} are only one order of magnitude lower. This sensitivity indicates that the surface diffusion is dominating the total flux. Figure 11 also shows that the temperature breakthrough curve (T'') at lower values of D_{so} is much different from that at higher values of D_{so}. Since the concentration front of propane is obscure at lower D_{so}, the hump of the temperature

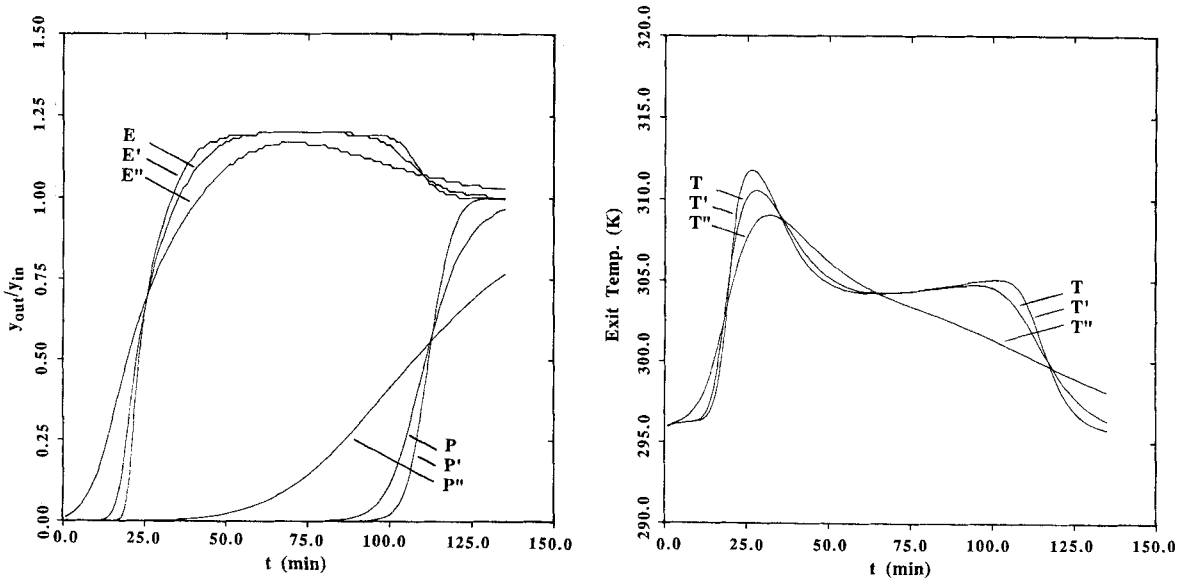

Figure 11. The influence of surface diffusivity D_{so} on the calculated breakthrough and temperature curves.
$D_{soe}/D_{sop} = 2 \times 10^{-4}/5 \times 10^{-4}(P, E, T)$, $D_{soe}/D_{sop} = 2 \times 10^{-3}/5 \times 10^{-3}(P', E', T')$, $D_{soe}/D_{sop} = 2 \times 10^{-5}/5 \times 10^{-5}(P'', E'', T'')$.

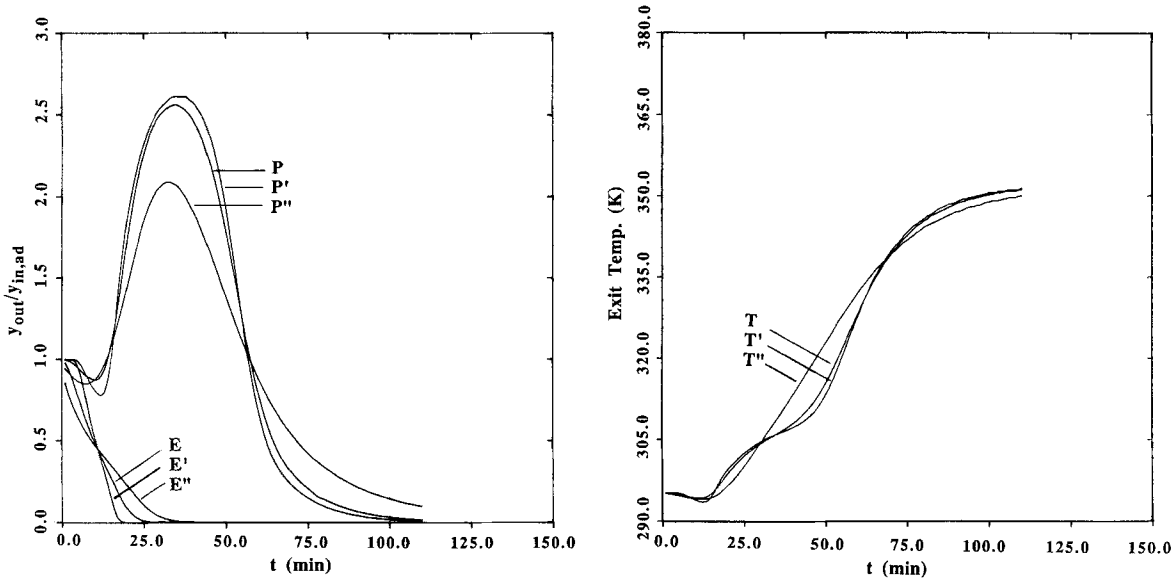

Figure 12. The influence of surface diffusivity D_{so} on the calculated depletion and temperature curves.
$D_{soe}/D_{sop} = 2 \times 10^{-4}/5 \times 10^{-4}(P, E, T)$, $D_{soe}/D_{sop} = 2 \times 10^{-3}/5 \times 10^{-3}(P', E', T')$, $D_{soe}/D_{sop} = 2 \times 10^{-5}/5 \times 10^{-5}(P'', E'', T'')$.

breakthrough curve, which is due to the heat of adsorption of propane, no longer appears.

Figures 13 to 16 show typical comparisons of experimental data and corresponding model results for bi-solute adsorption and regeneration processes. Figures 13 and 14 illustrate the breakthrough and depletion curves for a high propane inlet concentration (1.5%) run, using helium as the carrier and purge gas. Figures 15 and 16 illustrate the low propane inlet concentration (0.74%) cases, which used nitrogen as the carrier and purge gas. As can be seen, the model fits the experimental data very well, particularly for the concentration breakthrough and depletion curves. The scatter of temperatures recorded at the bottom of the bed (Figure 15) is due to the unstable thermocouple.

The roll-up heights of ethane predicted by the model are higher than those measured, for runs with nitrogen as carrier gas (see Figure 15). For the same runs the effluent concentrations of propane predicted by the model are lower than those measured. This is because nitrogen is competitive with the adsorbates even though its adsorbed amount is small. The adsorbed amount of carrier gas, however, is neglected in the model for simplifying purposes. This inert gas effect is more significant for the single-solute (ethane) run and is discussed later.

The predicted temperatures tracked the experimental temperature profiles, but with higher values. These differences can be explained in the following way. The radial heat conduction and heat conduction along the wall might be important in the

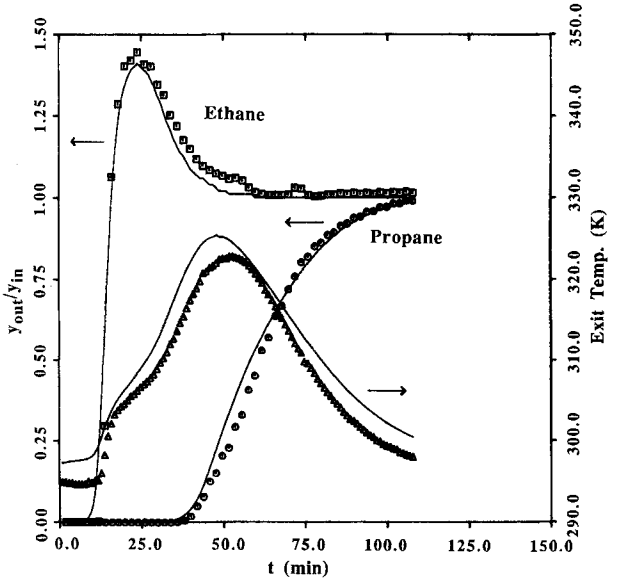

Figure 13. Simulation of experimental Run AD-8.
Carrier gas—helium. See Table 5 for operating conditions.

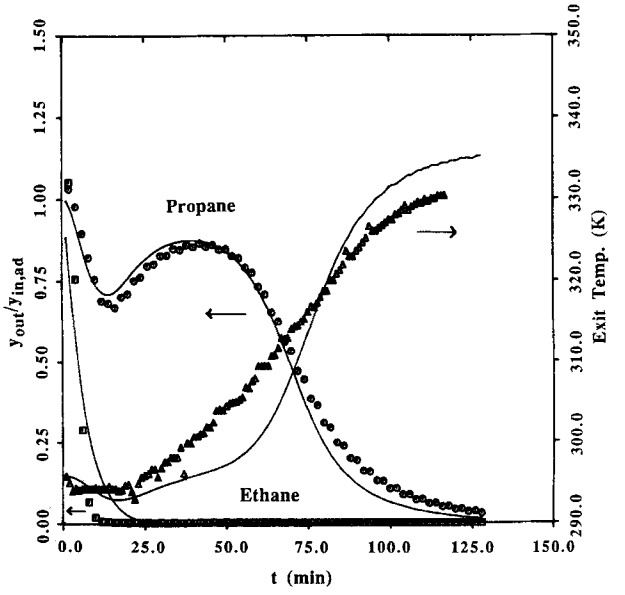

Figure 14. Simulation of experimental Run DE-8.
Purge gas—helium. See Table 5 for operating conditions.

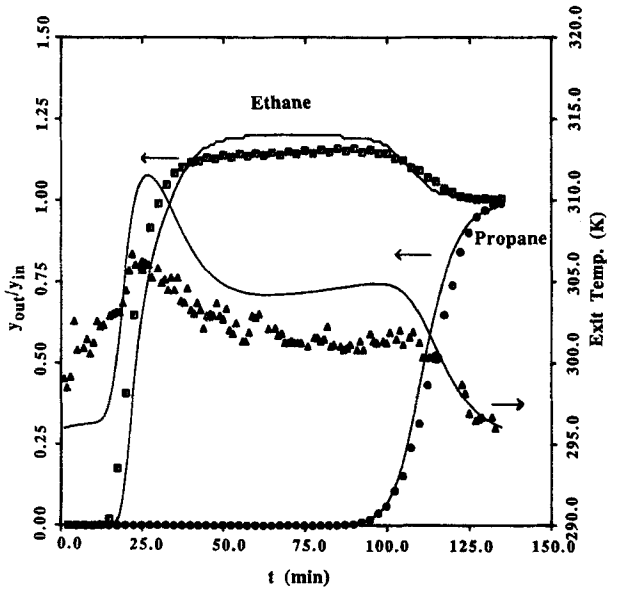

Figure 15. Simulation of experimental Run AD-22.
Carrier gas—nitrogen. See Table 5 for operating conditions.

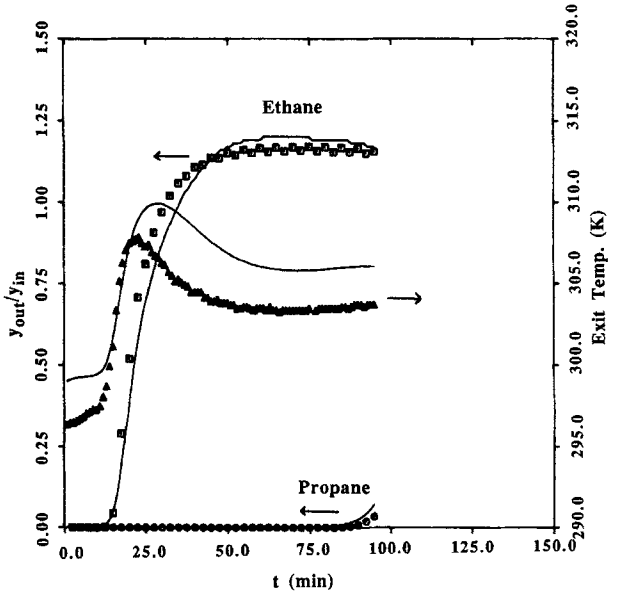

Figure 17. Simulation of experimental Run AD-21.
Carrier gas—nitrogen. See Table 5 for operating conditions.

apparatus used in the present study, but were neglected in the model. The heats of adsorption are functions of surface coverage, but were assumed constant in the whole range of operation.

Figures 17 and 18 show the comparisons of modeling results and experimental data for Run AD/DE-21. Adsorption was stopped at propane breakthrough. The simulation results compare well for the desorption step, indicating that the model may be used for simulating the regeneration of a partially saturated bed.

For single solute adsorption and desorption, simulation results along with experimental data are illustrated in Figures 19 and 20. The predicted values fit quite well although the predicted exit concentrations of ethane are lower than actual values. This is due to the use of nitrogen and its competition for the surface sites. Thus, the adsorbed amount of ethane is overpredicted and the complete regeneration time predicted by the model is longer than the actual time. In general, the model developed in this study applies both to multi-solute systems and single solute systems.

The sequential steps of adsorption run AD-27 and regeneration run DE-27 are simulated rather well, as shown in Figures 9 and 10. The instability of the ethane depletion curve in phase 2 is also predicted by the model. The predicted propane breakthrough curve in phase 2, however, is indicated by the experimental data. The depletion curves for regeneration shown in

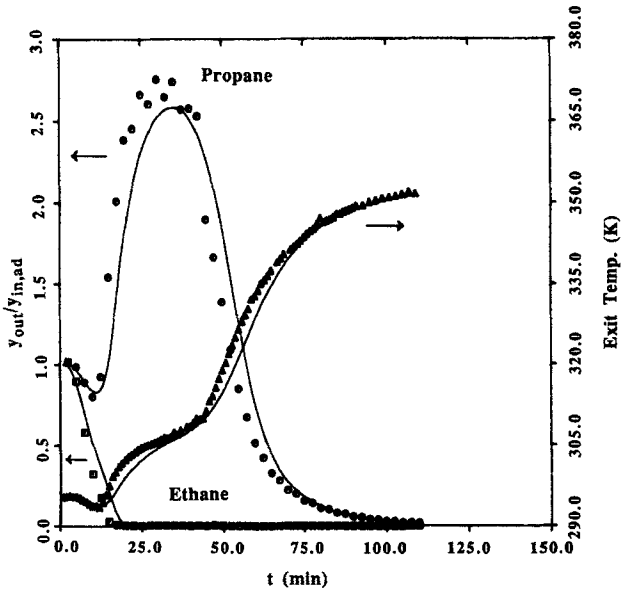

Figure 16. Simulation of experimental Run DE-22.
Purge gas—nitrogen. See Table 5 for operating conditions.

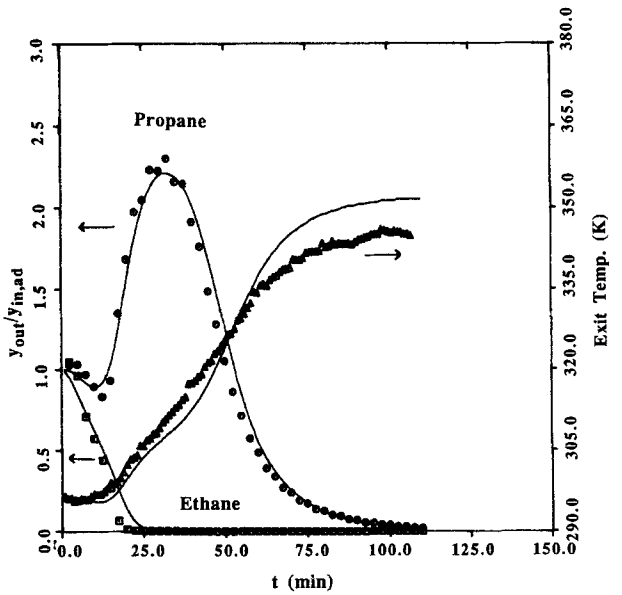

Figure 18. Simulation of experimental Run DE-21.
Purge gas—nitrogen. See Table 5 for operating conditions.

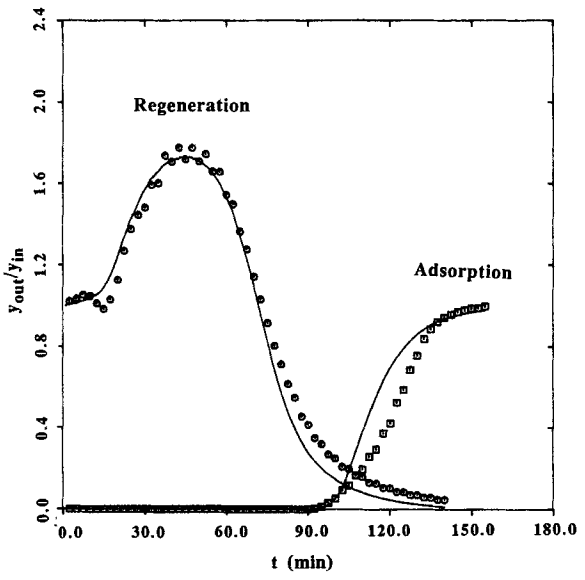

Figure 19. Simulation of experimental Run AD/DE-26.
Carrier and purge gas—helium. See Table 5 for operating conditions.

Figure 10 are more interesting. The depletion curve of propane resembles a chromatographic peak, which is also predicted quite well.

Conclusions

A nonequilibrium model has been developed for a nonisothermal, nonadiabatic fixed-bed adsorption and desorption cyclic process. A linear driving force mass transfer relationship with variable lumped-resistance coefficients provides a reasonable fit to measured adsorption and regeneration data. The Flory Huggins form of the vacancy solution model was used to predict mixture isotherms from pure component isotherms. The dynamic model simulates both single adsorbate and multiple adsorbate experiments well, even for sequential adsorption processes. This dynamic model also can simulate thermal swing adsorption cyclic processes with fully saturated or partially saturated adsorption steps.

Both adsorption and hot purge regeneration of the ethane/propane/activated carbon system are found to be intraparticle mass rate controlled processes. Surface diffusion dominates the intraparticle mass transfer mechanism.

The effluent concentration of the nonkey component (ethane) generally overshoots its inlet concentration during adsorption because of the displacement by the key component (propane). The effluent concentration of the key component generally overshoots its initial bed concentration during thermal regeneration.

Nitrogen is competitive with ethane for adsorption on activated carbon when the partial pressure of nitrogen is much higher than that of ethane. For isothermal operation, propane is a good regenerant for desorbing ethane, but ethane is not suitable for propane regeneration.

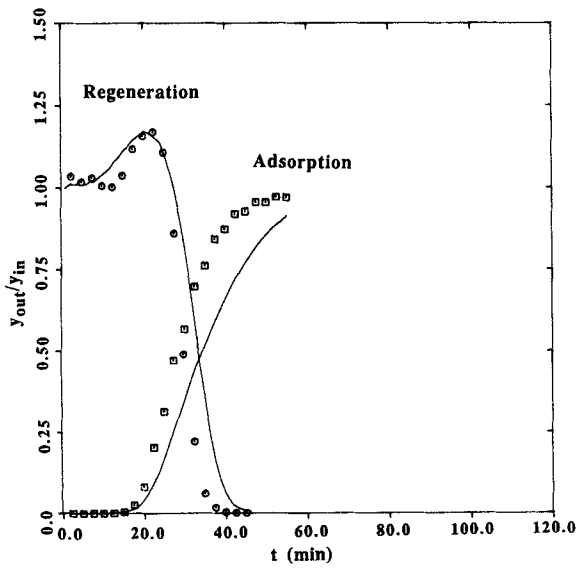

Figure 20. Simulation of experimental Run AD/DE-17.
Carrier and purge gas—nitrogen. See Table 5 for operating conditions.

Notation

b_i = Henry's law constant of ith component, kmol/kg · kPa
b_{0i} = temperature independent constant in Eq. 3
$c, \bar{c}_i^*$ = gas stream concentration, or gas phase concentration of ith component in equilibrium with w_i, kmol/m^3
c_{bi} = bulk phase concentration of ith component, kmol/m^3
$c_{ip}, \bar{c}_{ip}$ = gas-phase concentration, or volume average gas phase concentration of ith component in the pores of a particle, kmol/m^3
c_{pc}, c_{pg}, c_{ps} = heat capacity of column wall, gas phase, and solid particle, J/kg · K
c_{si} = gas phase concentration of ith component on the surface of particle pores, kmol/m^3
$c_{sur,i}$ = gas-phase concentration of ith component on the external particle surface, kmol/m^3
c_0, c_2 = constants in Eq. 21
D_{ij} = mutual diffusion coefficient of species i in binary of i and j, m^2/s
D_{im} = mutual diffusion coefficient of species i in mixture, m^2/s
D_{ki} = Knudsen diffusion coefficient of species i, m^2/s
D_{Li} = axial diffusion coefficient of species, i, m^2/s
$D_{pe,i}$ = effective diffusion coefficient of species i in porous media defined, m^2/s
D_{si} = surface diffusion coefficient of species i, m^2/s
$D_{so,i}$ = preexponential factor in the surface diffusion Eq. 13 of species i, m^2/s
E_{si} = surface diffusion energy of activation of species i
G = superficial molar gas flow rate, kmol/m^2 · s
h_f = heat transfer coefficient for gas film, J/m^2 · s · K
h_w = heat transfer coefficient for column wall, J/m^2 · s · K
(h_wA) = effective heat transfer coefficient times area in the end section of the column, J/s · K
$\Delta H_{ads}i, \Delta H_c$ = heat of adsorption of: adsorbate i, carrier gas, J/kmol
k_{ax} = axial thermal conductivity, J/m · s · K
k_{fi} = fluid film mass transfer coefficient of ith component, m/s
k_s = thermal conductivity of solid particle, J/m · s · K
$K_{eff,i}$ = effective mass transfer coefficient defined in Eq. 23, m/s
m = mass of sections at each end of adsorber, kg
m_1 = temperature independent constant in Eq. 4, kg/kmol
M_i = molecular weight of adsorbate i, kg/kmol
$N_{Re}, N_{Sc,i}$ = Reynolds number, Schmidt number of adsorbate i
N_{si} = molar flux along the solid surface, kmol/m^2 · s
P = pressure, kPa

r_e = mean pore radius, Å
r_1 = temperature independent constant in Eq. 2
R = gas constant, 8,314 J/kmol · K
t, t_s = time or stoichiometric breakthrough time, min
T_{amb}, T_{reg} = ambient temperature, regeneration temperature, K
T_c, T_g, T_s = temperature of column wall, gas phase, and solid phase, K
$(UA)_B$, $(UA)_T$ = effective heat transfer coefficient times area for the bottom, or top, section of the experimental equipment, J/s · K
U_{ins} = overall heat transfer coefficient for column insulation, J/m² · s · K
V = volume of end section of bed, m³
w_c, w_i = amount adsorbed of carrier gas or ith component, kmol/kg solid
w_i^∞ = limiting amount adsorbed of ith component, kmol/kg solid
w_{01}^∞ = temperature independent constant in Eq. 2, kmol/kg solid
x_i = mole fraction of ith component in adsorbed mixture
x_i^s = mole fraction of ith component in vacancy solution representing adsorbed phase
x_v^s = mole fraction of vacancy in vacancy solution
y_i, y_i^* = gas phase mole fraction of ith component, in equilibrium with w_i
z = axial position in the bed, m

Greek letters

α_c = ratio of the wall transfer area to wall volume defined as Eq. 28
α_{iv} = parameter of FH-VSM defined as Eq. 1
α_p = geometric surface area of cylindrical pellets, m⁻¹
γ_i^s = activity coefficient of ith component in adsorbed phase
ϵ_{ex} = external bed void volume
ϵ_p = particle porosity
θ = fraction of limiting adsorption defined as Eq. 5
ρ_b, ρ_c, ρ_p = bulk, column wall, and particle density, kg solid/m³ bed
τ_p, τ_s = pore, surface tortuosity factor
ϕ_i = fugacity coefficient of ith component in gas phase

Literature Cited

Aris, R., *Mathematical Theory of Diffusion and Reaction in Permeable Catalysts,* Vol. 1, Oxford University Press, London (1975).

Basmadjian, D., and P. Coroyannakis, "Equilibrium Theory Revisited. Isothermal Fixed-Bed Sorption of Binary Systems: I. Solutes Obeying the Binary Langmuir Isotherm," *Chem. Eng. Sci.,* **42**(7), 1723 (1987).

Basmadjian, D., P. Coroyannakis, and C. Carayanopoulos, "Equilibrium Theory Revisited. Isothermal Fixed-Bed Sorption of Binary Systems: II. Non-Langmuir Solutes with Type I Parent Isotherms: Azeotropic Systems," *Chem. Eng. Sci.,* **42**(7), 1737 (1987).

Basmadjian, D., C. Karayannopoulos, and P. Coroyannakis, "Equilibrium Theory Revisited. Isothermal Fixed-Bed Sorption of Binary Systems: III. Solutes with Type I, II and IV Parent Isotherms: Phase Separation Phenomena," *Chem. Eng. Sci.,* **42**(7), 1753 (1987).

Basmadjian, D., and D. W. Wright, "Nonisothermal Sorption of Ethane-Carbon Dioxide Mixtures in Beds of 5A Molecular Sieves," *Chem. Eng. Sci.,* **36,** 937 (1981).

Bird, R. B., W. E. Stewart, and E. N. Lightfoot, *Transport Phenomena,* Wiley, New York (1960).

Carter, J. W., and H. Husain, "The Simultaneous Adsorption of Carbon Dioxide and Water Vapor by Fixed Beds of Molecular Sieves," *Chem. Eng. Sci.,* **29,** 267 (1974).

Cochran, T. W., R. L. Kabel, and R. P. Danner, "Vacancy Solution Theory of Adsorption Using Flory-Huggins Activity Coefficient Equations," *AIChE J.,* **31**(2), 268 (Feb., 1985a).

———, "The Vacancy Solution Model of Adsorption Improvements and Recommendations," *AIChE J.,* **31**(12), 2075 (Dec., 1985b).

Collins, Jr., H. W., and K. C. Chao, "A Dynamic Model for Multicomponent Fixed Bed Adsorption," *AIChE Symp. Ser.,* **69**(134), 9 (1973).

Cooney, D. O., and F. P. Strusi, "Analytic Description of Fixed-Bed Sorption of Two Langmuir Solutes under Nonequilibrium Conditions," *Ind. Eng. Chem. Fund.,* **11**(1), 123 (1972).

Costa, E., G. Calleja, and F. Domingo, "Adsorption of Gaseous Hydrocarbons on Activated Carbon: Characteristic Kinetic Curve," *AIChE J.,* **31**(6), 982 (June, 1985).

Edwards, M. F., and J. F. Richardson, "Gas Dispersion in Packed Beds," *Chem. Eng. Sci.,* **23,** 109 (1968).

Gariepy, R. L., and I. Zwiebel, "Adsorption of Binary Mixtures in Fixed Beds," *AIChE Symp. Ser.,* **67**(117), 17 (1971).

Glueckauf, E., "Theory of Chromatography—Part 10," *Trans. Faraday Soc.,* **51,** 1540 (1955).

Grant, R. J., and M. Manes, "Adsorption of Binary Hydrocarbon Gas Mixtures on Activated Carbon," *Ind. Eng. Chem. Fundam.,* **5**(4), 490 (1966).

Harwell, J. H., A. I. Liapis, R. Litchfield, and D. T. Hanson, "A Non-Equilibrium Model for Fixed Multi-Component Adiabatic Adsorption," *Chem. Eng. Sci.,* **35,** 2287 (1980).

Huang, C.-C., "Thermal Regeneration of Fixed Multicomponent Adsorption Beds," Ph.D. Diss., Univ. of Texas at Austin (1987).

Kirk-Othmer, *Encyclopedia of Chemical Technology,* Vol. 12, Wiley, New York (1980).

Miura, K., and K. Hashimoto, "Analytical Solutions for the Breakthrough Curves of Bicomponent Fixed-Bed Adsorption under the Langmuir Isotherms," *J. Chem. Eng. Japan,* **12**(4), 329 (1979a).

Miura, K., H. Kurahashi, Y. Inokuchi, and K. Hashimoto, "A Method for Calculating Breakthrough Curves of Bicomponent Fixed-Bed Adsorption under Constant Pattern and Linear Driving Force," *J. Chem. Eng. Japan,* **12**(4), 281 (1979b).

Myers, A. L., "Adsorption of Pure Gases and Their Mixtures on Heterogeneous Surfaces," *Fundamentals of Adsorption* (Proc. of Eng. Foundation Conf. at Schloss Elmau, W. Germany, May, 1983), A. L. Myers, and G. Belfort, eds., United Eng. Trustees, New York, 365 (1984).

Myers, A. L., and J. M. Prausnitz, "Thermodynamics of Mixed-Gas Adsorption," *AIChE J.,* **11**(1), 121 (Jan., 1965).

Nagel, G., G. Kluge, and W. Flock, "Modelling of Non-Isothermal Multi-component Adsorption in Adiabatic Fixed Beds: I. The Numerical Solution of the Parallel Diffusion Model," *Chem. Eng. Sci.,* **42**(1), 143 (1987).

O'Brien, J. A., and A. L. Myers, "Rapid Calculations of Multi-Component Adsorption Equilibria from Pure Isotherm Data," *Ind. Eng. Chem. Process Des. Dev.,* **24,** 1188 (1985).

Petrovic, L. J., and G. Thodos, "Mass Transfer in the Flow of Gases through Packed Beds," *Ind. Eng. Chem. Fund.,* **7**(2), 274 (1968).

Rhee, H-K., and N. R. Amundson, "An Analysis of an Adiabatic Adsorption Column: Part I. Theoretical Development," *Chem. Eng. J.,* **1,** 241 (1970).

Rhee, H-K., E. D. Heerdt, and N. R. Amundson, "An Analysis of an Adiabatic Adsorption Column: Part III. Adiabatic Adsorption of Two Solutes," *Chem. Eng. J.,* **3,** 22 (1972).

Rhee, H-K., and N. R. Amundson, "Shock Layer in Two Solute Chromatography: Effect of Axial Dispersion and Mass Transfer," *Chem. Eng. Sci.,* **29,** 2049 (1974).

Ruthven, D. M., *Principles of Adsorption and Adsorption Processes,* Wiley, New York (1984).

Ruthven, D. M., K. F. Loughlin, and K. A. Holborow, "Multicomponent Sorption Equilibrium in Molecular Sieve Zeolites," *Chem. Eng. Sci.,* **28,** 701 (1973).

Satterfield, C. N., *Heterogeneous Catalysis in Practice,* McGraw-Hill, New York (1980).

———, *Mass Transfer in Heterogeneous Catalysis,* R. E. Krieger Publishing Co., Huntington, NY (1981).

Schork, J. M., "Thermal Regeneration of Fixed Adsorption Beds," Ph.D. Diss., Univ. of Texas at Austin (1986).

Schork, J. M., and J. R. Fair, "Parametric Analysis of Thermal Regeneration of Adsorption Beds," *Ind. Eng. Chem. Res.,* **27,** 457 (1988).

Schneider, P., and J. M. Smith, "Chromatographic Study of Surface Diffusion," *AIChE J.,* **14**(5), 886 (Oct., 1968).

Selwood, P. W., *Adsorption and Collective Paramagnetism,* Academic Press, New York (1962).

Sircar, S., and R. Kumar, "Adiabatic Adsorption of Bulk Binary Gas Mixtures: Analysis by Constant Pattern Model," *Ind. Eng. Chem. Process Des. Dev.,* **22,** 271 (1983).

———, "Equilibrium Theory for Adiabatic Desorption of Bulk Binary Gas Mixtures by Purge," *Ind. Eng. Chem. Process Des. Dev.*, **24**, 358 (1985).
———, "Column Dynamics for Adsorption of Bulk Binary Gas Mixtures on Activated Carbon," *Sep. Sci. Tech.*, **21**(9), 919 (1986).
Sircar, S., and A. L. Myers, "Surface Potential Theory of Multilayer Adsorption from Gas Mixtures," *Chem. Eng. Sci.*, **28**, 489 (1973).
Sladek, K. J., E. R. Gilliland, and R. F. Baddour, "Diffusion on Surfaces. II. Correlation of Diffusivities of Physically and Chemically Adsorbed Species," *Ind. Eng. Chem. Fund.*, **13**(2), 100 (1974).
Smith, J. M., *Chemical Engineering Kinetics*, 3rd ed., McGraw-Hill, New York (1981).
Suwanayuen, S., and R. P. Danner, "A Gas Adsorption Isotherm Equation Based on Vacancy Solution Theory," *AIChE J.*, **26**(1), 68 (Jan., 1980a).
———, "Vacancy Solution Theory of Adsorption from Gas Mixtures," *AIChE J.*, **26**(1), 76 (Jan., 1980b).
Szepesy, L., and V. Illés, "Adsorption of Gases and Gas Mixtures, I., II., III.," *Acta Chim. Hung.*, **35**, 37, 53, 245 (1963a, b, c).
Talu, O., and R. L. Kabel, "Isosteric Heat of Adsorption and the Vacancy Solution Model," *AIChE J.*, **33**(3), 510 (1987).
Thomas, W. J., and J. L. Lombardi, "Binary Adsorption of Benzene-Toluene Mixtures," *Trans. Instn. Chem. Engrs.*, **49**, 240 (1971).
Tsai, M. C., S. S. Wang, and R. T. Yang, "Pore Diffusion Model for Cyclic Separation," *AIChE J.*, **29**(6), 966 (Dec., 1983).
Wilke, C. R., "Diffusional Properties of Multicomponent Gases," *Chem. Eng. Prog.*, **46**(2), 95 (1950).
Wong, Y. W., and J. L. Niedzwiecki, "A Simplified Model for Multicomponent Fixed Bed Adsorption," *AIChE Symp. Ser.*, **78**(219), 120 (1982).
Yang, R. T., *Gas Separation by Adsorption Process*, Butterworths, Boston (1987).
Zwiebel, I., C. M. Kralik, and J. J. Schnitzer, "Fixed Bed Desorption Behavior of Gases with Nonlinear Equilibrium: Part II.," *AIChE J.*, **20**(5), 915 (Oct., 1974).

Manuscript received Nov. 13, 1987, and revision received June 1, 1988.